THE JOURNAL OF PHYSICAL CHEMISTRY C
A JOURNAL OF THE AMERICAN CHEMICAL SOCIETY

pubs.acs.org/JPCC

Article

Studies of the Reactivity of Graphene Driven by Mechanical Distortions

Nathaniel Hawthorne, Sayan Banerjee, Quentarius Moore, Andrew M. Rappe, and James D. Batteas*

Cite This: *J. Phys. Chem. C* 2022, 126, 17569−17578

Read Online

ACCESS | Metrics & More | Article Recommendations | Supporting Information

ABSTRACT: In mechanochemistry, the application of controlled forces is key to altering reaction rates and pathways to direct product yields and selectivity. However, a fundamental knowledge gap exists between what is occurring on the atomic scale in mechanically driven reactions and the resulting macroscale outcomes. Two-dimensional (2D) materials, such as graphene, proffer a model system to study the impact of mechanical forces, such as strain, on chemical reactivity, as force distributions may be applied across a well-organized atomic-scale structure comprising a single layer of C atoms. Here, using Raman micro-spectroscopy and first-principles calculations, we have investigated the reaction of graphene, under varying degrees of strain, with 4-nitrobenzenediazonium tetrafluoroborate (4-NBD). We find that only with increased out-of-plane distortion (shifting the C atoms of graphene from sp^2 toward sp^3 electronic states) would the reactivity be increased, with larger out-of-plane distortions yielding greater reactivity. Density functional theory (DFT) calculations reveal that increasing the curvature of graphene decreases the activation barrier of 4-NBD functionalization and enhances the thermodynamic favorability of the reaction. Furthermore, we find that curvature affects the orientation of the graphene $2p_z$ orbitals, and we then relate the thermodynamic feasibility of 4-NBD functionalization with the orbital orientation. These studies point to how the precise application of forces can be used to direct the functionalization of graphene for C−C bond forming reactions, which has significant implications for controlling its corresponding electronic structure in a well-defined fashion.

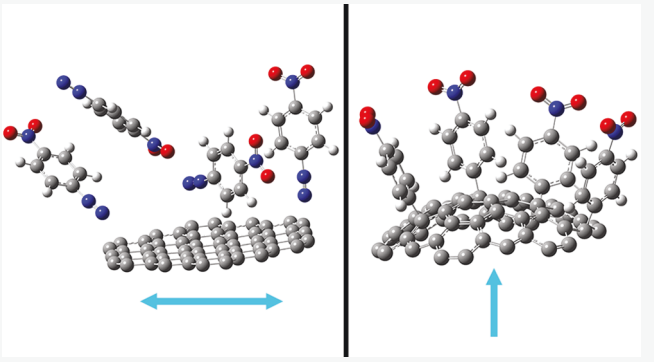

INTRODUCTION

The application of mechanical forces to surfaces has been shown to influence chemical reactivity in various ways, such as the breaking of surface bonds through applied shear that can lead to atomic scale wear.[1,2] Further, shearing under applied force has been demonstrated to help drive chemical reactions, such as in the case of the formation of tribofilms of zinc dialkyldithiophosphate (ZDDP) in base oils.[3] In such stress-assisted processes, a basic tenet of mechanochemistry is that the directionality of the applied force can influence which bonds are formed and/or broken.[4−6] Research in mechanochemistry has grown dramatically in recent years, with a host of reactions now known to be mechanically activated.[7−9] However, the complexity of the reaction conditions found in methods such as ball milling or twin-screw extrusion makes it challenging to explore fundamental mechanical questions such as how force directionality[10−12] controls selectivity and reactivity.

Two-dimensional (2D) materials such as graphene offer an ideal platform for the investigation of mechanochemical reactivity. Graphene, a 2D lattice of sp^2-hybridized carbon, has seen an explosion of interest in the research community since it was experimentally isolated in 2004.[13] It has found use in a variety of applications owing to its many unique properties, such as its high electrical conductivity,[14] high in-plane elastic moduli,[15] and low frictional properties.[16] Moreover, the ability to carry out directed functionalization of graphene opens the door to a host of exciting properties. For example, surface plasmon engineering can be achieved through patterning graphene with organic molecules[17] or through decorating graphene with Au nanostructures.[18] Functionalizing the π-surfaces of the layers in bulk graphite can cause delamination, leading to single-sheet graphene polyelectrolytes.[19] Furthermore, ferromagnetic and superparamagnetic behavior can be promoted in graphene through chemical functionalization.[20,21] In several of these applications, patterned functionalization on graphene is key; however, this remains a challenge.

While the basal plane of graphene is generally unreactive, incomplete bonding at interfaces can create strained regions

Received: July 25, 2022
Revised: September 21, 2022
Published: October 10, 2022

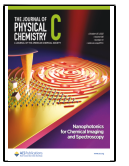

https://doi.org/10.1021/acs.jpcc.2c05261
J. Phys. Chem. C 2022, 126, 17569−17578

(including bond-angle strain), which can lead to mechanochemically accelerated oxidation and breakdown. Previous work has examined the breaking of C−F and C−O bonds on fluorinated and oxidized graphene using atomic force microscopy to investigate how such bond breaking depends on applied force.[22,23] Going the opposite way, fluorination, hydroxylation, and hydrogenation of graphene have been theoretically predicted to be more energetically favorable when the lattice is under compressive strain.[24] Functionalization with organic species has also been carried out using multi-pen arrays, such as Diels−Alder and Huisgen cycloaddition reactions through applied normal force,[25,26] enabling tracking of the kinetics of the reactions as a function of applied force and estimations of the reaction volumes.

The mechanical distortion of graphene when it conforms to any nonflat surface serves as an applied force directed across the lattice. In transition-state theory, a reaction can be envisioned as reactants moving along a potential energy surface, where the progress is quantified by movement along a reaction coordinate. The reaction coordinate serves as a representation of some change in the system, often the relative geometry of the reactants.[27] A potential energy surface has multiple reaction coordinates that the reaction may proceed along, based on which physical changes are relevant to the reaction (bond length, bond angle, etc.). The directed application of mechanochemical forces along the relevant reaction coordinate can help move the geometric state (i.e., the sp^2-lattice) of the reactant graphene closer to the configuration of the transition state (a mix of sp^2 and sp^3 character). In accordance with Hammond's postulate,[28] this deformation of graphene toward the transition state can thereby increase the rate and favorability of the reaction, e.g., the formation of out-of-plane C−C bonds.[29] To this end, the π-orbital axis vector (POAV) method[30−32] was developed to quantify the effect of distortion/strain on the π-orbitals for carbon atoms in conjugated aromatic compounds. It was hypothesized that mechanochemical strain can influence the electron delocalization as the orientation of the orbitals participating in the π-bond formation changes,[33] and recently, we demonstrated that POAV-derived quantities, such as the angle between two POAVs, can also explain kinetic barriers associated with molecular migration on curved graphene,[34] that others have experimentally observed, which can impact how aryl compounds either react to or migrate across, graphene surfaces.[35]

In the work presented here, we seek to elucidate the relationship between the magnitude and direction of applied mechanical strain on the graphene lattice and its ability to form out-of-plane C−C bonds. To investigate this, we examine the radical addition of 4-nitrobenzenediazonium tetrafluoroborate (4-NBD) to graphene, a model reaction of a diazonium salt with graphene that has been well examined in the literature, as a gauge of reactivity as a function of graphene strain.[33,36−45] For the reactions of graphene with diazonium molecules, it is proposed that the diazonium cation initially accepts an electron from the graphene lattice and generates an aryl radical upon releasing N_2.[36] This radical can then covalently bond to graphene, thereby changing the hybridization of the functionalized C center of graphene from sp^2 to sp^3. To further elucidate the influence of strain and curvature on the reactivity of graphene with 4-NBD, graphene has been deposited on flat silica substrates and on rough surfaces comprised of films of 6 nm in diameter silica nanoparticles to produce controlled graphene curvature, introduced by its conformal adhesion to the surface.

Using Raman spectroscopy, we found that the high curvature of the graphene induced via draping it over the silica nanoparticle film produced a significantly higher reactivity (ca. 2.7× that of the flat substrate) toward 4-NBD functionalization. Furthermore, we modeled the reactivity of graphene with 4-NBD using density functional theory calculations to determine the influence of the curvature of graphene on both the activation barrier for reaction and the overall reaction energy for functionalization. We then applied a descriptor[34] based on the POAV angle to understand the reactivity trend of graphene with little curvature, representative of being deposited on a flat surface, and graphene with varying curvature, representative of being deposited on films consisting of nanoparticles with variable diameters. The results presented herein may provide a guide for carrying out spatially controlled reactions on graphene through controlled lattice distortions.

EXPERIMENTAL METHODS

Fabrication of Substrates. Si(100) wafers (Virginia Semiconductor) were rinsed with nanopure H_2O (18.2 MΩ·cm, Barnstead) and ethanol (EtOH, 200 proof, Koptec) before being submerged in base piranha solution (4/1/1 v/v/v H_2O/conc. ammonium hydroxide (ACS Grade)/35 wt % hydrogen peroxide) at 85 °C for 20 min, re-rinsed with H_2O and EtOH, and dried with streaming N_2. For a 90 nm thermal oxide coating, samples were annealed at ambient pressure at 1050 °C for 1.5 h. For nanoparticle (NP) films, silica nanoparticle solutions (NexSil 6) were diluted down to 6 wt % with nanopure water. Then, 400−800 μL of the 6 wt % solutions was dispensed onto the cleaned Si(100) wafers, spin-coated for 1 min at 2000 rpm, and annealed at 500 °C for 5 h.

Depositing Graphene. The deposition of graphene on our substrates employed a method developed in-lab,[46] which was initially adapted from Song et al.[47] Briefly, CVD-grown graphene on Cu was purchased (LG), and polystyrene (PS−MW 13 000, Sigma-Aldrich) at 31.5 mg/mL in toluene was spin-coated onto the surface at 300 rpm for 2 min as a self-releasing layer. It was heated to 85 °C for 5 min to remove the solvent. A poly(dimethylsiloxane) (PDMS, Dow Inc.) stamp was placed on the PS-graphene stack and floated on an aqueous etchant solution (≈65 mM $Na_2S_2O_8$, Alfa Aesar) overnight to remove the Cu. The etchant solution was displaced with at least 1 L of nanopure water to rinse. The PDMS/PS/graphene stack was removed from the water, placed on the desired substrate, and dried in a vacuum desiccator. Upon drying, it was heated at 100 °C for 5 min to reach the T_g of PS, and the PDMS/PS was removed. The sample was immersed in toluene for ≈2 min to remove any residual PS from the surface.

Reacting Graphene Samples with 4-NBD. To examine reactivity, all samples were immersed in a solution of 11.5 mg/mL 4-NBD (TCI) in acetonitrile (ACS grade, VWR Analytical) for 10 min in a nitrogen tent (Captair Pyramid, Erlab) under dry conditions (<1% relative humidity). Vials containing the 4-NBD were wrapped in Al foil due to the light-sensitive nature of 4-NBD. After 10 min, the solution was poured off, and samples were immersed in separate vials of acetonitrile twice for ≈15 s each to remove any unreacted diazonium, then dried with streaming N_2.

Raman Spectroscopy. A WITec alpha300 RA confocal microscope equipped with an UHTS 300 VIS spectrometer

https://doi.org/10.1021/acs.jpcc.2c05261
J. Phys. Chem. C 2022, 126, 17569−17578

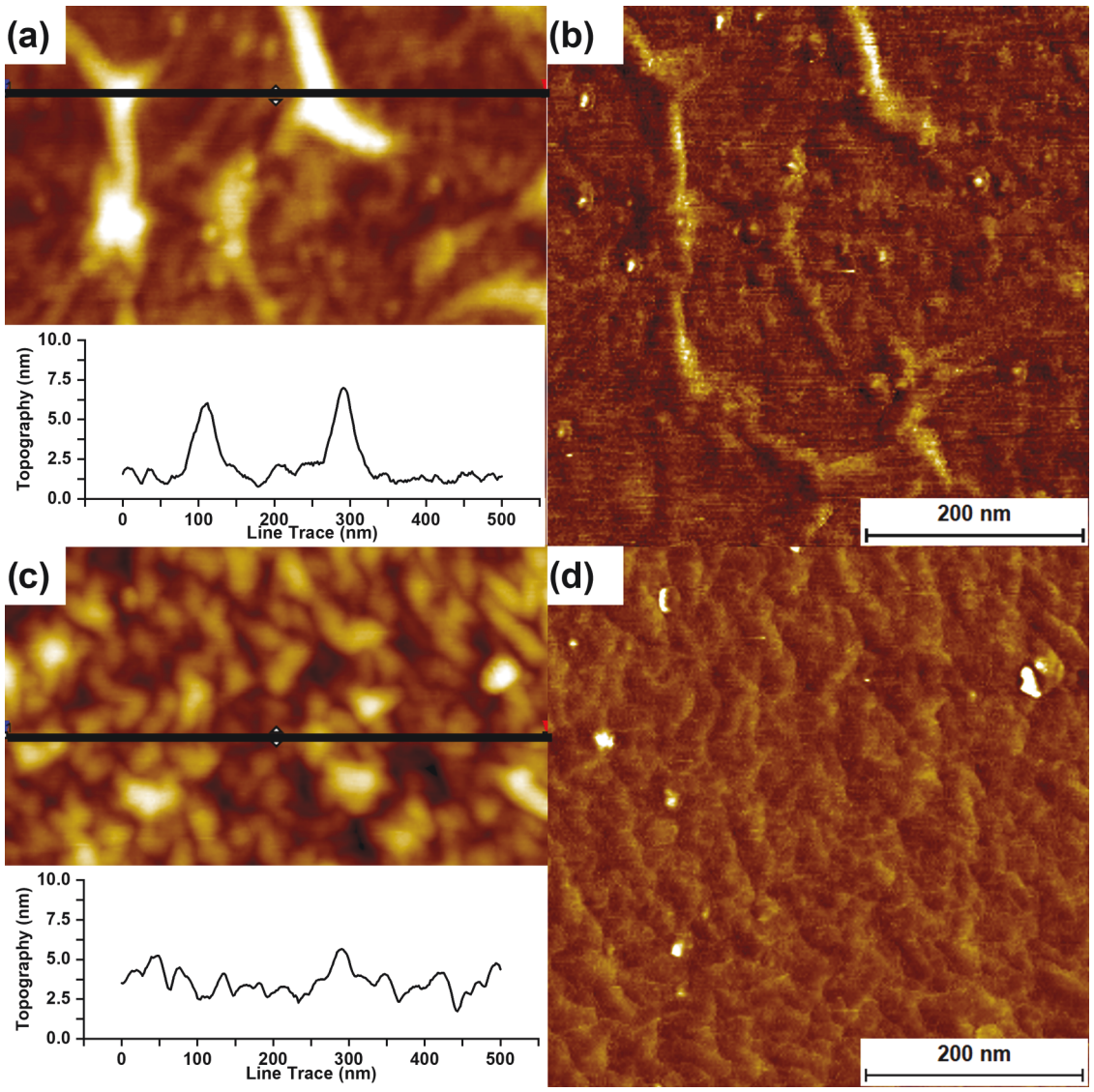

Figure 1. Representative tapping mode AFM images of SLG on flat silica (a) and 6 nm silica NP films (c), with inset corresponding line traces for each image. (b, d) Respective phase images for (a) and (c). On the flat surface, some wrinkles, folds, and blisters can appear.

and a cooled (−60 °C) Andor EMCCD detector was used for all Raman measurements. To avoid heating, measurements were taken with a 488 nm diode laser with a Nikon E Plan objective (100×, 0.9 NA) with power <1.25 mW on the surface. For all spectral maps, the 600 g/mm grating was used (resolution <3 cm^{-1}), and data were taken from 25 × 25 μm^2 areas consisting of 100 points/line, 100 lines/scan, and 0.1 s integration time per point. From each 25 × 25 μm^2 map, 3 spectra, each corresponding to the average over separate 5 × 5 μm^2 areas, were determined. Lorentz fits were applied to all peaks of these average spectra using Origin 2021 (OriginLab).

To determine the strain present in a given graphene lattice, the Lorentz fits of the G and 2D peak positions for each averaged area were compared to the Lorentz fits of the G and 2D peak position for suspended graphene using a method previously described in the literature.[48,49] Suspended graphene serves as a reference, as it is assumed to be nominally unstrained and undoped. This reference sample was made by transferring graphene onto a Si_3N_4 membrane with 1 μm diameter pores (Norcada) via the same transfer method used for the flat and NP films. Three Raman maps were then taken of the suspended graphene on the reference sample, each map 10 × 10 μm^2, consisting of 100 points/line, 100 lines/scan, and 0.15 s integration time per point. Average Raman spectra were extracted from the center 0.3 × 0.3 μm^2 of 60 suspended regions among the three maps. The unstrained, undoped G and 2D peak positions are calculated by averaging the Lorentz fit of these 60 regions (see Section 2 of the Supporting Information). All strain values in the main text were calculated using the equation in Section 3 of the Supporting Information.

To determine reactivity in the graphene films on flat and 6 nm silica NP films, the fits for the D and $-NO_2$ peaks were normalized to the Si peak (i.e., I_D/I_{Si} and I_{NO_2}/I_{Si}) and scaled using the average surface area ratios determined through atomic force microscopy (AFM) to account for the different amounts of graphene per unit area in the flat and NP samples imaged. While others have tracked the extent of reactivity on graphene by looking at the increase in the I_D/I_G ratio, we chose to scale relative to I_{Si}, as the G peak width, size, and location can be affected by exposure to the diazonium,[33,43,50] and as the extent of out-of-plane bond formation increases, the intensity

https://doi.org/10.1021/acs.jpcc.2c05261
J. Phys. Chem. C 2022, 126, 17569−17578

of the D′ peak increases, which has partial overlap with the G peak.[43]

Atomic Force Microscopy. An Agilent 5500 AFM was used for surface roughness measurements and scratch tests. Surface roughness and surface area measurements were conducted as 500 × 500 nm^2 scans in a nitrogen environment (0.1% relative humidity) using tips coated with diamond-like carbon (125 μm cantilever, DLC, Budget Sensors) in tapping mode. Scratch tests were also conducted in a nitrogen environment (0.1% relative humidity) using silicon tips (300−350 μm cantilevers, HQ:CSC37, MikroMasch) in contact mode. Initial and post-scratch scans were performed at 1 nN at scan sizes 1 × 1 μm^2 and greater, and the scratch tests occurred at 20 nN as 500 × 500 nm^2 scans. The surface roughness and surface area values were determined, and all images were processed using the software program Scanning Probe Image Processing (SPIP version 6.7.2). The Sader method[51] was used to determine the spring constants *in situ* for the scratch tests. Tip radii were determined using $SrTiO_3$ to reverse-image the tips, and a parabolic fit was applied to determine the radius of curvature[52] using Origin 2021. The tapping mode tips ranged from 17 to 21 nm, and the contact mode tips after the scratch tests ranged from 21 to 40 nm radius of curvature.

Computational Methods. Density functional theory (DFT) calculations were performed using the Quantum ESPRESSO software package.[53] The kinetic barriers were calculated using the climbing image nudged elastic band method.[54] We used a 6 × 6 supercell of graphene to understand the effect of curvature on the 4-NBD functionalization trend. A Γ-centered 3 × 3 × 1 *k*-point grid had been implemented to sample the Brillouin zone. A vacuum size of 20 Å was implemented between the graphene slabs along *z*-axis to minimize any artificial interaction between the periodic images. Electronic exchange−correlation energy was calculated using the generalized gradient approximation.[55] Designed, optimized, norm-conserving, and nonlocal pseudopotentials were generated using the OPIUM (version 3.7) software.[56−58] The energy cutoff used was 50 Ry to expand the valence electron wave functions in the plane-wave basis. Further, we used the DFT-D3 dispersion correction to capture the dispersion and noncovalent interactions.[59,60]

RESULTS AND DISCUSSION

In our prior studies and in others, it has been shown that the extent to which graphene conforms to a substrate is dependent on the substrate roughness and the relative interaction strength of the graphene with the substrate.[61−64] Furthermore, the reactivity of graphene has been shown to be strongly influenced by substrate interactions.[43] For the silica surfaces employed here, graphene tends to conform more tightly to surfaces with lower roughness. This enables us to control the extent of conformity based on the size of the nanoparticle features on the surface. Thus, depositing graphene on a film made of small (6 nm) nanoparticles engenders tighter conformity through the application of a combination of uniaxial and biaxial strain, leading to out-of-plane distortions. On the other hand, graphene on flat silica has a significantly lower extent of out-of-plane distortion, although some wrinkles and blisters were observed.

We performed tapping mode AFM under dry conditions (0.1% relative humidity) to determine the surface roughness and conformity of graphene on various silica films. Representative AFM images of graphene on the flat and nanoparticle silica films are shown in Figure 1. For graphene on flat silica (Figure 1a), we find occasional wrinkles and blisters with localized height increases stemming from incomplete adhesion of graphene to the flat surface. On average, 88 ± 7% of the surface is free of wrinkles and blisters (see Table S1 and Figure S1). Graphene appears to conform tightly on the 6 nm NP films (Figure 1c), with some areas draped between nearby nanoparticles. We found that in each sample type, there is little variation in the surface roughness among the measured areas and that within each measurement, there is greater height variation for SLG on 6 nm NPs vs on flat SiO_2 (see Figure S1 and Tables S1 and S2). As expected, the RMS roughness of graphene on the 6 nm NP films (1.10 ± 0.02 nm) is slightly higher than that on the flat silica (0.9 ± 0.1 nm), similar to prior work.[61]

To understand the out-of-plane curvature of graphene on the NP films, we first measured the surface area of graphene-covered 6 nm silica NP films and flat silica films using AFM scans of identical size. Then, the surface area ratio was calculated by comparing the average surface area of graphene on the NP films to the average surface area of graphene on flat silica (Table S2). We find that there is ≈0.2% more graphene present on the NP films than flat silica as a result of the conformity to the NPs, inducing the out-of-plane curvature.

The strain and doping present in a given graphene lattice can be estimated by a correlation analysis method,[48] which compares the Raman G and 2D peak positions between a given sample and an optimal unstrained, undoped sample of graphene.[49] The unstrained and undoped G and 2D peak positions ($\omega_G{}^0$ and $\omega_{2D}{}^0$, respectively) are calculated by averaging the Lorentz fit of the average G and 2D peak positions for 60 regions of graphene suspended over 1 μm pores in a Si_3N_4 membrane and found to be 1585.9 ± 2.3 and 2684.6 ± 4.1 cm^{-1}, respectively (see Figures S2 and S3 for a representative Raman spectrum and the peak positions of each measured area).

The G and 2D peak positions (ω_G and ω_{2D}) of graphene on the 6 nm NP silica films and on the flat silica are shown in Figure 2. Along with the peak locations, lines are marked to indicate the predicted peak positions for undoped graphene

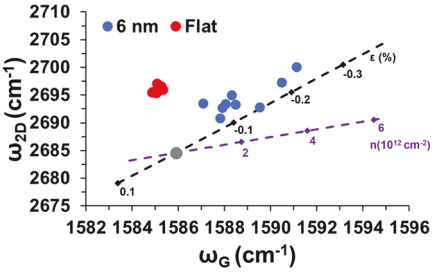

Figure 2. 2D and G peak positions for graphene on 6 nm silica NPs (blue) and flat silica (red) substrates. The gray dot is the average peak location of the suspended reference. To guide the eyes, lines have been added to indicate the expected peak positions for only strained graphene with no doping (black) and only doped graphene with no strain (purple), referenced to our experimental suspended graphene average values. The black diamonds indicate an increase in compressive strain in 0.1% increments as ω_G increases and an increase in tensile strain in 0.1% increments as ω_G decreases. The purple diamonds indicate an increase in p-type doping in 2 × 10^{12} cm^{-2} increments.

https://doi.org/10.1021/acs.jpcc.2c05261
J. Phys. Chem. C 2022, 126, 17569−17578

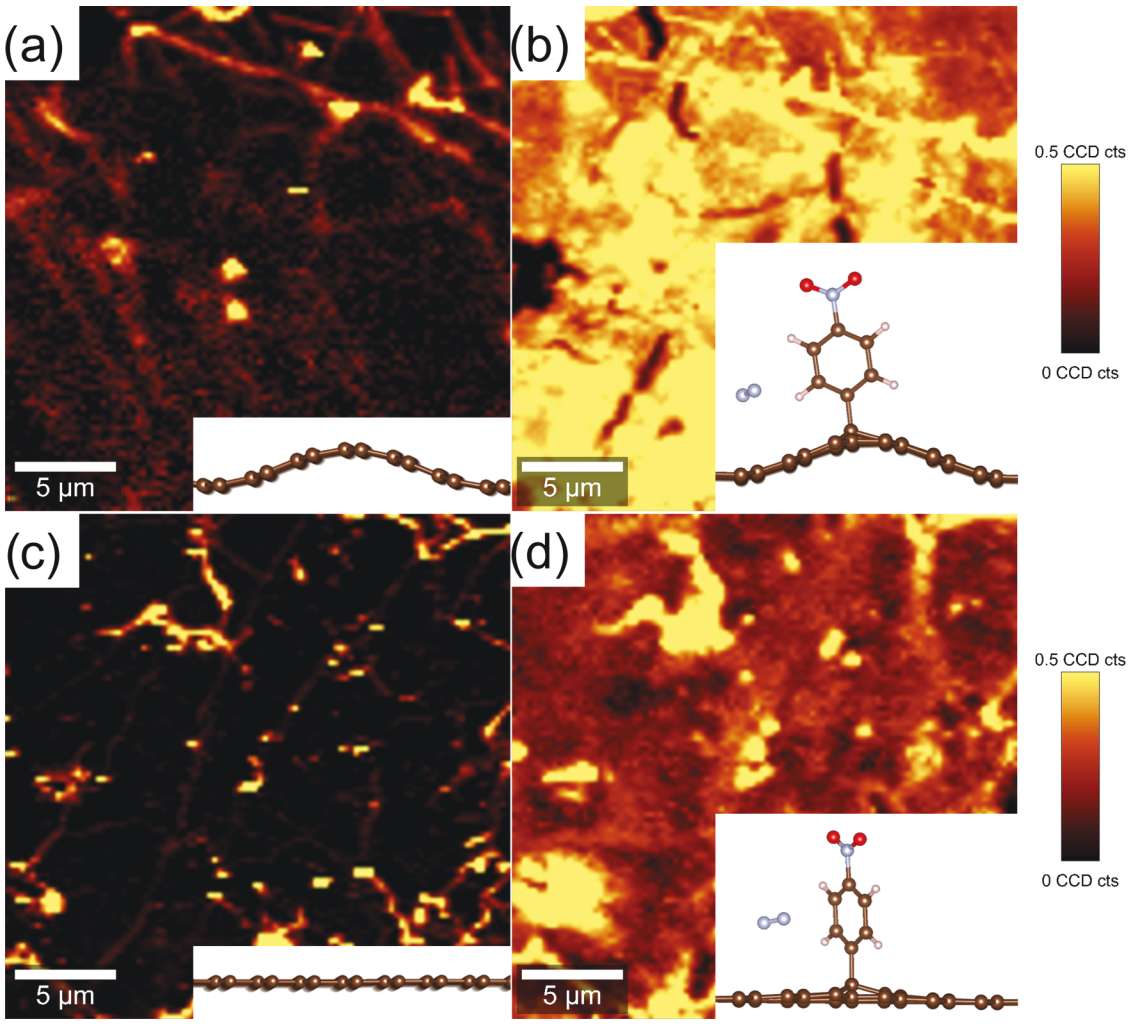

Figure 3. Raman spectral maps of the graphene D peak (presented as total spectral intensity from 1310 to 1410 cm^{-1}) normalized to the height of the Si peak (located ≈523 cm^{-1}) of the underlying substrate. Maps are of graphene on 6 nm silica NP films and on flat silica before (a, c) and after (b, d) functionalization with the 11.5 mg/mL solution of 4-NBD in acetonitrile. Insets are molecular models of the curved and flat graphene before and after reacting with 4-NBD.

under variable degrees of strain (black) and unstrained graphene under variable amounts of doping (purple) based on our ω_G^0 and ω_{2D}^0, using the values of $(\Delta\omega_{2D}/\Delta\omega_G)_\varepsilon = 2.2$ and $(\Delta\omega_{2D}/\Delta\omega_G)_\eta = 0.7$, from literature.[48] Furthermore, the gray dot is the location average position for our suspended graphene. The peak positions for graphene on flat silica are tightly clustered together compared to the peak positions for graphene on the 6 nm NPs, indicating a lower degree of strain variation in the graphene lattice when on a flat surface. On the other hand, the graphene on the NP films has rich spatial heterogeneity in the initial peak positions, which is indicative of strain variation at the localized interface across the sample surface.

The peak positions track closely with the predicted positions for graphene that is strained but undoped, indicating that strain is the more important factor in these samples. It has been previously reported that wrinkles can be generated in chemical vapor deposition-grown graphene due to the mismatch in the thermal expansion coefficient between graphene and Cu and hence can also be induced in the graphene lattice while transferring it to a substrate.[65] These additional wrinkles can lead to variation in peak positions for both the flat and nanoparticle silica films. Thus, in this regard, it is better to focus more on the qualitative trends present in reactivity and the Raman-derived strain values.

We calculated the average uniaxial areal strain for 5 × 5 μm^2 areas of graphene on nanoparticle silica films using the equation from Zhang et al.[49] and our experimental ω_G^0 and ω_{2D}^0 values for the suspended graphene as a reference (see Sections 2 and 3 of the Supporting Information). The correlation analysis method calculates strain as uniaxial,[48,49] and although the actual strain present in the graphene lattice when on a substrate is a combination of uniaxial and biaxial due to geometric frustration of the lattice,[66,67] the magnitude would not vary significantly, since the calculated strain is areal in nature (the change in area, not of length in one direction).[49]

After all of the samples were exposed to 11.5 mg/mL 4-NBD in acetonitrile for an identical amount of time, Raman spectra were taken again at the same locations that were used to determine the initial strain. As can be seen in the Raman maps showing just the D peak spectral intensity before and after exposure to 4-NBD (Figure 3), the graphene on the flat surface is far less reactive than the strained graphene on the 6 nm NP films. Representative Raman spectra are displayed in Figure 4. As the sp^3-hybridized carbon introduces defects in the planar sp^2-hybridized graphene architecture, the intensity of the

https://doi.org/10.1021/acs.jpcc.2c05261
J. Phys. Chem. C 2022, 126, 17569−17578

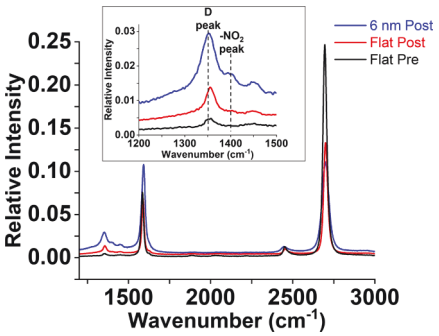

Figure 4. Representative Raman spectra of graphene on a 6 nm silica NP film and flat silica after reacting with 4-NBD compared to graphene on flat silica before the reaction occurs. Inset is the region where the growth in the D and $-NO_2$ peak positions are located. Peak intensities are relative to the height of the Si peak centered around 523 cm^{-1} (peak not shown).

Raman D peak can be used to quantify the extent of 4-NBD functionalization.

While most of the literature on the reaction of graphene and 4-NBD follows the growth of the D peak as an indicator of reactivity,[36−40,42,44,45,68] the diazonium compound itself also has a peak (≈1335 cm^{-1}) that can spectrally overlap with the graphene D peak signal.[69] Here, we investigate whether the growth of the $-NO_2$ asymmetric stretch peak from the nitro functional group on the diazonium[42,68,70] at ≈1400 cm^{-1} can also be monitored to track the extent of the reaction.

The growth of both peaks was observed, and to normalize across samples, the increase in the intensity of the peaks relative to the intensity of the Si peak from the underlying substrates was scaled using the average surface area ratio determined through AFM to account for the different concentrations of graphene per unit area among the flat and NP samples exposed to the laser beam (Table S2). Note that while the surface area ratio was determined from 500 × 500 nm^2 AFM scans, a series of length-scale measurements indicated it does not change up to 5 × 5 μm^2 (Figure S4), making it a viable scaling factor to apply to the Raman peak intensities.

From the representative spectra in Figure 4, graphene on the 6 nm NP films reacted to a greater extent with the diazonium compound than graphene on flat silica, indicated by an increase in both the D and $-NO_2$ peaks. For all areas sampled, the increase of reactivity, $\Delta(I_D/I_{Si})$ and $\Delta(I_{NO_2}/I_{Si})$, is plotted against the initial strain (Figure 5). Note that the negative values correspond to compressive strain, while positive values would represent tensile strain, indicating all samples are more compressive in nature than the suspended reference.

From Figure 5, every area of graphene sampled on the 6 nm NP films reacted to a greater extent than all areas of graphene on flat silica, indicated both by larger D and $-NO_2$ peaks, although not all areas on flat silica had an $-NO_2$ peak that could be observed above the spectral baselines. Taking just the D peak as an indicator, the relative increase in reactivity on the NP film was found to be ca. 2.7 ± 0.9 times greater than on the flat surface. The strain in the graphene on the NP film was largely 0.10−0.20% more tensile than the average strain in the graphene on flat silica, and the increase in strain stemmed from the graphene lattice conforming to the out-of-plane features of the nanoparticles vs the flat silica. Thus, it is the out-of-plane curvature that is correlated to the increased reactivity, similar

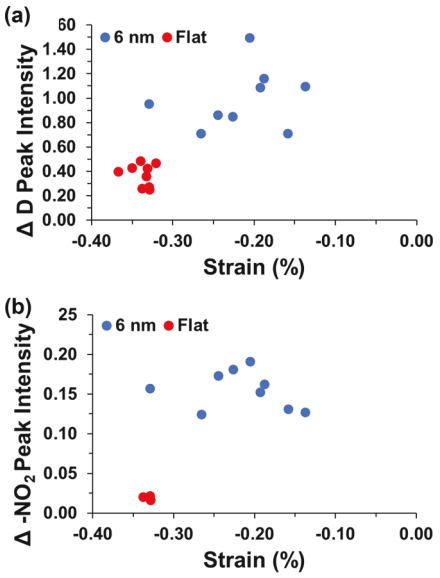

Figure 5. (a) I_D/I_{Si} growth rate, $[(I_D/I_{Si})_{post} - (I_D/I_{Si})_{pre}]$ and (b) I_{NO_2}/I_{Si} growth rate, $[(I_{NO_2}/I_{Si})_{post} - (I_{NO_2}/I_{Si})_{pre}]$ vs initial average uniaxial strain for graphene on 6 nm NP silica (blue) and flat silica (red).

to what has been observed for the increased reactivity of 4-NBD with graphene when it was deposited over isolated silica nanoparticles.[44] Our results differ, however, from a prior study of graphene deposited on poly(dimethylsiloxane) (PDMS), where in-plane tensile strain was introduced to the graphene lattice by stretching the PDMS support.[45] In these studies, the authors reported up to a ca. 1.64× increase in graphene reactivity under in-plane strain. However, as a result of slippage, the strain in the support is not necessarily the same as the strain in the graphene lattice itself, and so a direct comparison to our work cannot be made.

Lastly, while there have been reports of 4-NBD reacting with itself and forming polymer chains extending from the graphitic surface,[37,71] that was not seen here. After functionalizing the samples, contact mode AFM scratch tests were performed to see if a polymer film of the diazonium was present and could be removed. Each type of sample was scratched with a 20 nN applied load, and there was little to no change in topography or friction (Figures S5 and S6) beyond a minimal decrease in topography for graphene on flat silica (Figure S6) attributed to the flattening of wrinkles and blisters. These results indicated that no polymer film of the diazonium was formed on top of the graphene.

To better understand the atomistic origin of the curvature effect on the reactivity of graphene with the diazonium species, we performed plane-wave density functional theory (DFT) calculations. To achieve curvature in the lattice, flat sheets of graphene were compressed in one dimension in a way so that the diameters (d) of the curved/rippled graphene (see Figure S7) correspond to the experimentally used nanoparticle diameter. Here, we approximate that the diameter of the rippled graphene corresponds to the nanoparticle diameter. To confirm the validity of the systems with 1D curvature in explaining the energetics of graphene functionalization on a support with variable nanoparticle diameters, we additionally performed classical Molecular Dynamics (MD) simulations to model flat graphene (see Section 6.2 in the Supporting Information) and graphene indented by a sphere of 6 nm

https://doi.org/10.1021/acs.jpcc.2c05261
J. Phys. Chem. C 2022, 126, 17569−17578

diameter in two dimensions, which corresponded to 2D curvature of graphene. We found that the energies of formation for the reaction of graphene with 4-NBD in both 1D and 2D curvature models can be fitted in a single model when plotted against the radius of curvature at the functionalized center of the distorted graphene lattice (Figure S9). Thus, we found that both 1D and 2D models provide similar information regarding the curvature effect on reactivity. Overall, we show that the model of 1D rippling can capture the reactivity trend of graphene deposited on spherical nanoparticles with different diameters (Figures S7 and S9). We further conclude that the 4-NBD functionalization of graphene mostly depends on the local electronic and geometric environment, as both the 1D and 2D curvature analysis for graphene provide the same reactivity trend (Figure S9). The details regarding two different models are given in the Supporting Information (see Section 6.2 and Figure S9).

Note that the data presented in the next paragraphs correspond to the 1D curvature model. Using that model, we calculated the activation energy for graphene 4-NBD functionalization vs the diameter of its templating silica nanoparticle, as shown in Figure 6.

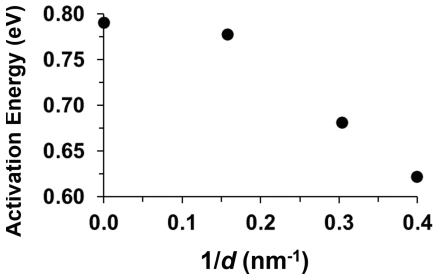

Figure 6. Activation barrier for graphene 4-NBD functionalization vs the inverse of the diameter of the silica nanoparticle taken from the 1D model. We approximate that the graphene deposited on the nanoparticle has the same diameter as the nanoparticle. $1/d = 0$ corresponds to flat graphene.

Here, we found that the activation barrier decreases as the diameter of the substrate silica nanoparticle (d) decreases, indicating the 4-NBD functionalization becomes kinetically more facile as the curvature of graphene increases. For a 6 nm nanoparticle, the corresponding $1/d$ value is 0.17 nm^{-1}, and the activation barrier decreased to 0.78 from 0.79 eV for $1/d$ = 0. As the data in Figure 6 correspond to 1D curvature and do not consider solvent effects, potential contamination, or saturation of bonding sites, we emphasize the qualitative trend over exact quantitative accuracy. To further confirm the trend theoretically, additional data points calculated with $1/d$ values of 0.3 and 0.4 nm^{-1} are considered (the rightmost two points in Figure 6). We find that the activation barrier decreases to 0.68 and 0.62 eV for $1/d$ = 0.3 and 0.4 nm^{-1}, respectively, which further confirms our observation that graphene conformed to a smaller diameter nanoparticle would result in increased out-of-plane reactivity. The qualitative trend observed in the calculations, i.e., 4-NBD functionalization becomes more facile as the NP diameter decreases, can also be seen for the larger growth of the D and $-NO_2$ peaks of graphene on 6 nm NPs vs flat silica in Figure 5.

For a quasi-quantitative comparison, we further estimated the relative reaction rate constants between graphene on the 6 nm NP films and on flat silica by applying the Arrhenius equation to the activation energies in Figure 6 through eq 1

$$k_6/k_{flat} = \exp(-E_{A,6}/k_B T)/\exp(-E_{A,flat}/k_B T) \quad (1)$$

where k is the reaction rate constant, E_A is the calculated activation barrier, k_B is the Boltzmann constant, and T is room temperature (293 K).

From Table 1, the experimental relative reactivity for the I_D/I_{Si} of graphene on 6 nm NPs to graphene on flat silica is slightly higher than the calculated k_6/k_{flat} (2.7 ± 0.9 vs 1.5). Note that the calculated k_6/k_{flat} does not consider solvent effects, potential contamination, or saturation of bonding sites. As previously stated, the symmetric $-NO_2$ peak[69] is generally found around 1320−1360 cm^{-1} for 4-NBD. We were unable to separate its effect from our D peak fit. Likely, the true I_D/I_{Si} ratio for graphene on 6 nm NPs to graphene on flat silica would be somewhat lower, putting it in line with the calculated k_6/k_{flat}.

Table 1. Relative Reactivity Comparison for Graphene Deposited on 6 nm NP vs Flat Silica Films Computationally and Experimentally

	relative reactivity
calculated k_6/k_{flat}	1.5
experimental $\Delta(I_D/I_{Si})_{ave\ 6}/\Delta(I_D/I_{Si})_{ave\ flat}$	2.7 ± 0.9
experimental $\Delta(I_{NO_2}/I_{Si})_{ave\ 6}/\Delta(I_{NO_2}/I_{Si})_{ave\ flat}$	8 ± 2

The estimated relative reactivity from the I_{NO_2}/I_{Si} of graphene on 6 nm NPs to graphene on flat silica is ≈3 to 5 times higher than that indicated by the growth of the D peak and the reaction rate constants. In the literature, the asymmetric $-NO_2$ peak ≈1400 cm^{-1} is usually assigned to physisorbed 4-NBD in the form of a charge-transfer complex.[42,72,73] Our AFM scratch tests did not show a change of friction after high load scans, indicating that no physisorbed or polymerized material was being sheared away from on top of the surface (Figures S5 and S6). However, due to how much higher the estimated relative reactivity appears to be from the I_{NO_2}/I_{Si} for graphene on 6 nm NP films vs graphene on flat silica is than that determined through the other indicators, it is likely that there is unreacted 4-NBD trapped under the graphene and between the 6 nm NP film, and to a lesser extent, under the graphene on the flat silica. Any unreacted diazonium under the SLG would still generate a Raman signal but would be unlikely to cause a significant difference in friction in AFM as it is under the features being probed. This is further supported by how few of the graphene on flat silica samples exhibited any $-NO_2$ peak at ≈1400 cm^{-1}, whereas all of the graphene on 6 nm NP films did; it is easier for the diazonium to get trapped between particles than between two flat surfaces. Based on this, while the growth of the $-NO_2$ peak at ≈1400 cm^{-1} indicates the presence of diazonium, it is a less robust method than the traditional approach of monitoring the growth of the D peak for the reactivity of graphene.

Next, as we found that the geometric structure of the transition state (TS) of 4-NBD functionalization corresponds mainly to the N_2 dissociation rather than the C−C bond formation between the diazonium and graphene (see Figure S10), this observation suggests that the interaction between 4-NBD and graphene does not play the central role in determining the activation barrier. However, we do find that

https://doi.org/10.1021/acs.jpcc.2c05261
J. Phys. Chem. C 2022, 126, 17569−17578

the functionalization step is concerted in nature, i.e., both $-N_2$ dissociation and C−C bond formation happen at a single step, and no intermediate exists for this reaction. Interestingly, we find that the activation energy is strongly correlated with the energy of formation (ΔE) with R^2 of 0.93 (Figure S11) and thus follows the Bell−Evans−Polanyi (BEP) principle. Such BEP correlation suggests that the reactivity trend (and the rate) can be understood from the reaction thermodynamics. We found that the initial state, which is the curved graphene with unbound 4-NBD, rises in energy as the curvature increases and becomes more like the transition-state geometry. This leads to a decrease of activation barrier (Figure 6), in line with Hammond's postulate.[28,29]

To further understand the origin of the destabilization of curved graphene in comparison to flat graphene, we construct a theoretical model based on POAV approach (shown in Figure 7b, here, $\vec{V}_\pi$ is the POAV) developed previously.[30−32]

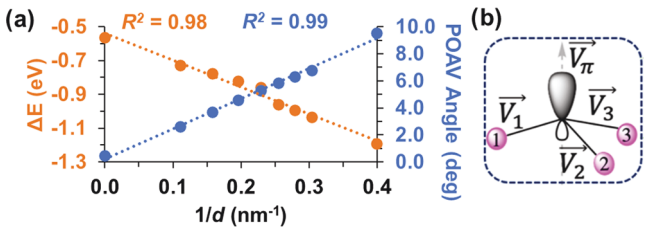

Figure 7. (a) Energy of formation (ΔE, orange) and the π-orbital axis vector angle (POAV, blue) vs the inverse of the diameter of the silica nanoparticle. We approximate that the graphene deposited on the nanoparticle has the same diameter as the nanoparticle. (b) Schematic indicating the direction of the POAV ($\vec{V}_\pi$), which depends on the local coordination environment and bond vectors ($\vec{V}_1$, $\vec{V}_2$, and $\vec{V}_3$).

According to the POAV analysis, the carbon atom π-orbitals in locally distorted conjugated organic species experience greater chemical reactivity due to the decreased π electron delocalization.[30−32] The angle between the two adjacent POAVs is defined as "POAV angle," which has been shown to capture the effect of local curvature on molecular migration barriers on curved graphene.[34] Here, we have adapted the POAV angle descriptor approach to understand the ΔE trends as a function of nanoparticle diameter. Specifically, we use the POAV angle between the $2p_z$ orbitals of the curved graphene near the region of 4-NBD functionalization center (Figure 7a) such that a higher POAV angle value corresponds to more distortion from a planar sp^2 graphene structure. More details regarding the calculation of the POAV angle are given in the Supporting Information (Section 6.6). We have created a grid by varying the nanoparticle diameter and found that both the ΔE and POAV angle correlate linearly with $1/d$ (orange and blue lines in Figure 7a). As we have shown that the activation energy and ΔE are linearly correlated for 4-NBD functionalization (Figure S11), studying the ΔE trend should also provide insight into the kinetics. The positive correlation between $1/d$ and ΔE (orange line in Figure 7a) indicates that graphene deposited on smaller diameter nanoparticle substrates should have greater reactivity toward 4-NBD functionalization, supporting our experimental observations (Figure 5 and Table 1). Further, we find that $1/d$ has a positive correlation with the POAV angle, suggesting that graphene deposited on a lower diameter silica nanoparticle has a higher POAV angle (blue line in Figure 7a) and, thus, less in-plane electron delocalization. A lesser extent of in-plane electron delocalization allows the availability of the electrons near the Fermi energy and therefore increases the reactivity toward out-of-plane functionalization. Hence, we conclude that as a result of higher curvature, the in-plane electron delocalization of graphene due to the π-bonding decreases and ultimately results in an increased out-of-plane reactivity. Our theoretical results explain the role of curvature on the reactivity of graphene, and this method of correlating POAV angle, energy of formation, and curvature can be extended to elucidate the reactivity of other 2D materials.

CONCLUSIONS

Overall, we have studied the aryl radical reaction between 4-NBD and graphene and elucidated the role of out-of-plane curvature on the reactivity of graphene. Theoretical investigations further delineate how curvature affects the frontier orbital orientation of graphene and thereby modulates the reactivity toward out-of-plane 4-NBD functionalization. Our experimental and theoretical results derived from considering graphene as a model system for studying mechanical deformation will provide insights into connecting the atomistic causes of mechanochemical reactions with the macroscale results. Moreover, the results presented here underpin the promise of exploring the curvature effect on the reactivity of other 2D materials of interest.

ASSOCIATED CONTENT

Supporting Information

The Supporting Information is available free of charge at https://pubs.acs.org/doi/10.1021/acs.jpcc.2c05261.

Additional experimental results, including the average roughness of graphene on various substrates, an explanation of strain calculations, prereaction size series surface area information, post-reaction AFM scratch test images, and an explanation and comparison of computational methods (PDF)

AUTHOR INFORMATION

Corresponding Author

James D. Batteas − *Department of Chemistry, Texas A&M University, College Station, Texas 77843-3255, United States; Department of Materials Science and Engineering, Texas A&M University, College Station, Texas 77843-3003, United States;* orcid.org/0000-0002-6244-5000; Email: batteas@chem.tamu.edu

Authors

Nathaniel Hawthorne − *Department of Chemistry, Texas A&M University, College Station, Texas 77843-3255, United States*

Sayan Banerjee − *Department of Chemistry, University of Pennsylvania, Philadelphia, Pennsylvania 19104-6323, United States;* orcid.org/0000-0002-8586-9236

Quentarius Moore − *Department of Chemistry, Texas A&M University, College Station, Texas 77843-3255, United States*

Andrew M. Rappe − *Department of Chemistry, University of Pennsylvania, Philadelphia, Pennsylvania 19104-6323, United States; Department of Materials Science and Engineering, University of Pennsylvania, Philadelphia, Pennsylvania 19104-6272, United States;* orcid.org/0000-0003-4620-6496

Complete contact information is available at:

https://doi.org/10.1021/acs.jpcc.2c05261
J. Phys. Chem. C 2022, 126, 17569−17578

https://pubs.acs.org/10.1021/acs.jpcc.2c05261

Author Contributions

The manuscript was written through contributions of all authors. N.H. performed the experiments with guidance from J.D.B. S.B. and Q.M. carried out the theoretical calculations with guidance from A.M.R. All authors have given approval to the final version of the manuscript.

Notes

The authors declare no competing financial interest.

■ ACKNOWLEDGMENTS

This work was supported by the NSF Center for the Mechanical Control of Chemistry under Grant # CHE-2023644. S.B. acknowledges the Vagelos Institute for Energy Science and Technology for the graduate fellowship. Q.M. acknowledges support from a DOE Computational Science Graduate Fellowship.

■ REFERENCES

(1) Jacobs, T. D. B.; Gotsmann, B.; Lantz, M. A.; Carpick, R. W. On the Application of Transition State Theory to Atomic-Scale Wear. *Tribol. Lett.* **2010**, *39*, 257−271.
(2) Jacobs, T. D. B.; Carpick, R. W. Nanoscale Wear as a Stress-Assisted Chemical Reaction. *Nat. Nanotechnol.* **2013**, *8*, 108−112.
(3) Gosvami, N. N.; Bares, J. A.; Mangolini, F.; Konicek, A. R.; Yablon, D. G.; Carpick, R. W. Mechanisms of Antiwear Tribofilm Growth Revealed in situ by Single-Asperity Sliding Contacts. *Science* **2015**, *348*, 102−106.
(4) Konôpka, M.; Turanský, R.; Reichert, J.; Fuchs, H.; Marx, D.; Štich, I. Mechanochemistry and Thermochemistry are Different: Stress-Induced Strengthening of Chemical Bonds. *Phys. Rev. Lett.* **2008**, *100*, No. 115503.
(5) Davis, D. A.; Hamilton, A.; Yang, J.; Cremar, L. D.; Van Gough, D.; Potisek, S. L.; Ong, M. T.; Braun, P. V.; Martínez, T. J.; White, S. R.; et al. Force-Induced Activation of Covalent Bonds in Mechanoresponsive Polymeric Materials. *Nature* **2009**, *459*, 68−72.
(6) Black, A. L.; Lenhardt, J. M.; Craig, S. L. From Molecular Mechanochemistry to Stress-Responsive Materials. *J. Mater. Chem.* **2011**, *21*, 1655−1663.
(7) Friščić, T.; Mottillo, C.; Titi, H. M. Mechanochemistry for Synthesis. *Angew. Chem., Int. Ed.* **2020**, *59*, 1018−1029.
(8) Tan, D.; García, F. Main Group Mechanochemistry: from Curiosity to Established Protocols. *Chem. Soc. Rev.* **2019**, *48*, 2274−2292.
(9) Mateti, S.; Mathesh, M.; Liu, Z.; Tao, T.; Ramireddy, T.; Glushenkov, A. M.; Yang, W.; Chen, Y. I. Mechanochemistry: A Force in Disguise and Conditional Effects Towards Chemical Reactions. *Chem. Commun.* **2021**, *57*, 1080−1092.
(10) Andersen, J. M.; Mack, J. Decoupling the Arrhenius Equation via Mechanochemistry. *Chem. Sci.* **2017**, *8*, 5447−5453.
(11) Burmeister, C. F.; Kwade, A. Process Engineering with Planetary Ball Mills. *Chem. Soc. Rev.* **2013**, *42*, 7660−7667.
(12) Do, J.-L.; Friščić, T. Mechanochemistry: A Force of Synthesis. *ACS Cent. Sci.* **2017**, *3*, 13−19.
(13) Novoselov, K. S.; Geim, A. K.; Morozov, S. V.; Jiang, D.; Zhang, Y.; Dubonos, S. V.; Grigorieva, I. V.; Firsov, A. A. Electric Field Effect in Atomically Thin Carbon Films. *Science* **2004**, *306*, 666−669.
(14) Du, X.; Skachko, I.; Barker, A.; Andrei, E. Y. Approaching Ballistic Transport in Suspended Graphene. *Nat. Nanotechnol.* **2008**, *3*, 491−495.
(15) Lee, C.; Wei, X.; Kysar, J. W.; Hone, J. Measurement of the Elastic Properties and Intrinsic Strength of Monolayer Graphene. *Science* **2008**, *321*, 385−388.
(16) Lin, L.-Y.; Kim, D.-E.; Kim, W.-K.; Jun, S.-C. Friction and Wear Characteristics of Multi-Layer Graphene Films Investigated by Atomic Force Microscopy. *Surf. Coat. Technol.* **2011**, *205*, 4864−4869.
(17) Cheng, J.; Wang, W. L.; Mosallaei, H.; Kaxiras, E. Surface Plasmon Engineering in Graphene Functionalized with Organic Molecules: A Multiscale Theoretical Investigation. *Nano Lett.* **2014**, *14*, 50−56.
(18) Bianco, G. V.; Giangregorio, M. M.; Losurdo, M.; Sacchetti, A.; Capezzuto, P.; Bruno, G. Demonstration of Improved Charge Transfer in Graphene/Au Nanorods Plasmonic Hybrids Stabilized by Benzyl Thiol Linkers. *J. Nanomater.* **2016**, *2016*, No. 2561326.
(19) Swager, T. M. Functional Graphene: Top-Down Chemistry of the π-Surface. *ACS Macro Lett.* **2012**, *1*, 3−5.
(20) Wei, W.; Qu, X. Extraordinary Physical Properties of Functionalized Graphene. *Small* **2012**, *8*, 2138−2151.
(21) López-Urías, F.; Martínez-Iniesta, A. D.; Morelos-Gómez, A.; Muñoz-Sandoval, E. Tuning the Electronic and Magnetic Properties of Graphene Nanoribbons through Phosphorus Doping and Functionalization. *Mater. Chem. Phys.* **2021**, *265*, No. 124450.
(22) Raghuraman, S.; Elinski, M. B.; Batteas, J. D.; Felts, J. R. Driving Surface Chemistry at the Nanometer Scale Using Localized Heat and Stress. *Nano Lett.* **2017**, *17*, 2111−2117.
(23) Felts, J. R.; Oyer, A. J.; Hernández, S. C.; Whitener Jr, K. E.; Robinson, J. T.; Walton, S. G.; Sheehan, P. E. Direct Mechanochemical Cleavage of Functional Groups from Graphene. *Nat. Commun.* **2015**, *6*, No. 6467.
(24) Boukhvalov, D. W.; Son, Y.-W. Covalent Functionalization of Strained Graphene. *ChemPhysChem* **2012**, *13*, 1463−1469.
(25) Bian, S.; Scott, A. M.; Cao, Y.; Liang, Y.; Osuna, S.; Houk, K. N.; Braunschweig, A. B. Covalently Patterned Graphene Surfaces by a Force-Accelerated Diels−Alder Reaction. *J. Am. Chem. Soc.* **2013**, *135*, 9240−9243.
(26) Han, X.; Bian, S.; Liang, Y.; Houk, K. N.; Braunschweig, A. B. Reactions in Elastomeric Nanoreactors Reveal the Role of Force on the Kinetics of the Huisgen Reaction on Surfaces. *J. Am. Chem. Soc.* **2014**, *136*, 10553−10556.
(27) Fukui, K. Formulation of the reaction coordinate. *J. Phys. Chem. A* **1970**, *74*, 4161−4163.
(28) Hammond, G. S. A Correlation of Reaction Rates. *J. Am. Chem. Soc.* **1955**, *77*, 334−338.
(29) Haddon, R. C.; Chow, S. Y. Hybridization as a Metric for the Reaction Coordinate of Chemical Reactions. *J. Am. Chem. Soc.* **1998**, *120*, 10494−10496.
(30) Haddon, R. C. Hybridization and the Orientation and Alignment of π-orbitals in Nonplanar Conjugated Organic Molecules: π-Orbital Axis Vector Analysis (POAV2). *J. Am. Chem. Soc.* **1986**, *108*, 2837−2842.
(31) Haddon, R. C. Pyramidalization: Geometrical Interpretation of the π-Orbital Axis Vector in Three Dimensions. *J. Phys. Chem. B* **1987**, *91*, 3719−3720.
(32) Haddon, R. C. Rehybridization and π-Orbital Overlap in Nonplanar Conjugated Organic Molecules: π-Orbital Axis Vector (POAV) Analysis and Three-Dimensional Hueckel Molecular Orbital (3D-HMO) Theory. *J. Am. Chem. Soc.* **1987**, *109*, 1676−1685.
(33) Bekyarova, E.; Sarkar, S.; Wang, F.; Itkis, M. E.; Kalinina, I.; Tian, X.; Haddon, R. C. Effect of Covalent Chemistry on the Electronic Structure and Properties of Carbon Nanotubes and Graphene. *Acc. Chem. Res.* **2013**, *46*, 65−76.
(34) Banerjee, S.; Rappe, A. M. Mechanochemical Molecular Migration on Graphene. *J. Am. Chem. Soc.* **2022**, *144*, 7181−7188.
(35) He, M.; Swager, T. M. Aryl Migration on Graphene. *J. Am. Chem. Soc.* **2020**, *142*, 17876−17880.
(36) Chua, C. K.; Pumera, M. Covalent Chemistry on Graphene. *Chem. Soc. Rev.* **2013**, *42*, 3222−3233.
(37) Greenwood, J.; Phan, T. H.; Fujita, Y.; Li, Z.; Ivasenko, O.; Vanderlinden, W.; Van Gorp, H.; Frederickx, W.; Lu, G.; Tahara, K.; et al. Covalent Modification of Graphene and Graphite Using Diazonium Chemistry: Tunable Grafting and Nanomanipulation. *ACS Nano* **2015**, *9*, 5520−5535.

(38) Huang, P.; Jing, L.; Zhu, H.; Gao, X. Diazonium Functionalized Graphene: Microstructure, Electric, and Magnetic Properties. *Acc. Chem. Res.* **2013**, *46*, 43−52.
(39) Paulus, G. L. C.; Wang, Q. H.; Strano, M. S. Covalent Electron Transfer Chemistry of Graphene with Diazonium Salts. *Acc. Chem. Res.* **2013**, *46*, 160−170.
(40) Solís-Fernández, P.; Bissett, M. A.; Tsuji, M.; Ago, H. Tunable Doping of Graphene Nanoribbon Arrays by Chemical Functionalization. *Nanoscale* **2015**, *7*, 3572−3580.
(41) Sinitskii, A.; Dimiev, A.; Corley, D. A.; Fursina, A. A.; Kosynkin, D. V.; Tour, J. M. Kinetics of Diazonium Functionalization of Chemically Converted Graphene Nanoribbons. *ACS Nano* **2010**, *4*, 1949−1954.
(42) Fan, X.-Y.; Nouchi, R.; Yin, L.-C.; Tanigaki, K. Effects of Electron-Transfer Chemical Modification on the Electrical Characteristics of Graphene. *Nanotechnology* **2010**, *21*, No. 475208.
(43) Wang, Q. H.; Jin, Z.; Kim, K. K.; Hilmer, A. J.; Paulus, G. L.; Shih, C. J.; Ham, M. H.; Sanchez-Yamagishi, J. D.; Watanabe, K.; Taniguchi, T.; et al. Understanding and Controlling the Substrate Effect on Graphene Electron-Transfer Chemistry via Reactivity Imprint Lithography. *Nat. Chem.* **2012**, *4*, 724−732.
(44) Wu, Q.; Wu, Y.; Hao, Y.; Geng, J.; Charlton, M.; Chen, S.; Ren, Y.; Ji, H.; Li, H.; Boukhvalov, D. W.; et al. Selective Surface Functionalization at Regions of High Local Curvature in Graphene. *Chem. Commun.* **2013**, *49*, 677−679.
(45) Bissett, M. A.; Konabe, S.; Okada, S.; Tsuji, M.; Ago, H. Enhanced Chemical Reactivity of Graphene Induced by Mechanical Strain. *ACS Nano* **2013**, *7*, 10335−10343.
(46) Negrito, M.; Elinski, M. B.; Hawthorne, N.; Pedley, M. P.; Han, M.; Sheldon, M.; Espinosa-Marzal, R. M.; Batteas, J. D. Using Patterned Self-Assembled Monolayers to Tune Graphene−Substrate Interactions. *Langmuir* **2021**, *37*, 9996−10005.
(47) Song, J.; Kam, F.-Y.; Png, R.-Q.; Seah, W.-L.; Zhuo, J.-M.; Lim, G.-K.; Ho, P. K. H.; Chua, L.-L. A General Method for Transferring Graphene onto Soft Surfaces. *Nat. Nanotechnol.* **2013**, *8*, 356−362.
(48) Lee, J. E.; Ahn, G.; Shim, J.; Lee, Y. S.; Ryu, S. Optical Separation of Mechanical Strain from Charge Doping in Graphene. *Nat. Commun.* **2012**, *3*, No. 1024.
(49) Zhang, Y.; Heiranian, M.; Janicek, B.; Budrikis, Z.; Zapperi, S.; Huang, P. Y.; Johnson, H. T.; Aluru, N. R.; Lyding, J. W.; Mason, N. Strain Modulation of Graphene by Nanoscale Substrate Curvatures: A Molecular View. *Nano Lett.* **2018**, *18*, 2098−2104.
(50) Das, A.; Pisana, S.; Chakraborty, B.; Piscanec, S.; Saha, S. K.; Waghmare, U. V.; Novoselov, K. S.; Krishnamurthy, H. R.; Geim, A. K.; Ferrari, A. C.; Sood, A. K. Monitoring Dopants by Raman Scattering in an Electrochemically Top-Gated Graphene Transistor. *Nat. Nanotechnol.* **2008**, *3*, 210−215.
(51) Sader, J. E.; Chon, J. W. M.; Mulvaney, P. Calibration of Rectangular Atomic Force Microscope Cantilevers. *Rev. Sci. Instrum.* **1999**, *70*, 3967−3969.
(52) Sheiko, S. S.; Möller, M.; Reuvekamp, E. M. C. M.; Zandbergen, H. W. Calibration and Evaluation of Scanning-Force-Microscopy Probes. *Phys. Rev. B* **1993**, *48*, 5675−5678.
(53) Giannozzi, P.; Baroni, S.; Bonini, N.; Calandra, M.; Car, R.; Cavazzoni, C.; Ceresoli, D.; Chiarotti, G. L.; Cococcioni, M.; Dabo, I.; et al. QUANTUM ESPRESSO: a Modular and Open-Source Software Project for Quantum Simulations of Materials. *J. Phys.: Condens. Matter* **2009**, *21*, No. 395502.
(54) Henkelman, G.; Uberuaga, B. P.; Jónsson, H. A Climbing Image Nudged Elastic Band Method for Finding Saddle Points and Minimum Energy Paths. *J. Chem. Phys.* **2000**, *113*, 9901−9904.
(55) Perdew, J. P.; Burke, K.; Ernzerhof, M. Generalized Gradient Approximation Made Simple. *Phys. Rev. Lett.* **1996**, *77*, 3865−3868.
(56) Rappe, A. M.; Rabe, K. M.; Kaxiras, E.; Joannopoulos, J. D. Optimized Pseudopotentials. *Phys. Rev. B* **1990**, *41*, 1227−1230.
(57) Ramer, N. J.; Rappe, A. M. Designed Nonlocal Pseudopotentials for Enhanced Transferability. *Phys. Rev. B* **1999**, *59*, 12471−12478.
(58) Yang, J. Opium − Pseudopotential Generation Project. http://opium.sourceforge.net/index.html (accessed September 14, 2021).
(59) Grimme, S.; Antony, J.; Ehrlich, S.; Krieg, H. A Consistent and Accurate ab initio Parametrization of Density Functional Dispersion Correction (DFT-D) for the 94 elements H-Pu. *J. Chem. Phys.* **2010**, *132*, No. 154104.
(60) Moellmann, J.; Grimme, S. DFT-D3 Study of Some Molecular Crystals. *J. Phys. Chem. C* **2014**, *118*, 7615−7621.
(61) Elinski, M. B.; Liu, Z.; Spear, J. C.; Batteas, J. D. 2D or not 2D? The Impact of Nanoscale Roughness and Substrate Interactions on the Tribological Properties of Graphene and MoS_2. *J. Phys. D: Appl. Phys.* **2017**, *50*, No. 103003.
(62) Spear, J. C.; Custer, J. P.; Batteas, J. D. The Influence of Nanoscale Roughness and Substrate Chemistry on the Frictional Properties of Single and Few Layer Graphene. *Nanoscale* **2015**, *7*, 10021−10029.
(63) Goncher, S. J.; Zhao, L.; Pasupathy, A. N.; Flynn, G. W. Substrate Level Control of the Local Doping in Graphene. *Nano Lett.* **2013**, *13*, 1386−1392.
(64) Lee, C.; Li, Q.; Kalb, W.; Liu, X.-Z.; Berger, H.; Carpick, R. W.; Hone, J. Frictional Characteristics of Atomically Thin Sheets. *Science* **2010**, *328*, 76−80.
(65) Deng, S.; Berry, V. Wrinkled, Rippled and Crumpled Graphene: An Overview of Formation Mechanism, Electronic Properties, and Applications. *Mater. Today* **2016**, *19*, 197−212.
(66) Grason, G. M.; Davidovitch, B. Universal Collapse of Stress and Wrinkle-to-Scar Transition in Spherically Confined Crystalline Sheets. *Proc. Natl. Acad. Sci. U.S.A.* **2013**, *110*, 12893.
(67) Zhou, Y.; Chen, Y.; Liu, B.; Wang, S.; Yang, Z.; Hu, M. Mechanics of Nanoscale Wrinkling of Gaphene on a Non-Developable Surface. *Carbon* **2015**, *84*, 263−271.
(68) Zhu, H.; Huang, P.; Jing, L.; Zuo, T.; Zhao, Y.; Gao, X. Microstructure Evolution of Diazonium Functionalized Graphene: A Potential Approach to Change Graphene Electronic Structure. *J. Mater. Chem.* **2012**, *22*, 2063−2068.
(69) Sampathkumar, K.; Diez-Cabanes, V.; Kovaricek, P.; del Corro, E.; Bouša, M.; Hošek, J.; Kalbac, M.; Frank, O. On the Suitability of Raman Spectroscopy to Monitor the Degree of Graphene Functionalization by Diazonium Salts. *J. Phys. Chem. C* **2019**, *123*, 22397−22402.
(70) El'kin, P. M.; Pulin, V. F.; Kosterina, E. K. Structural Dynamic Models and Vibrational Spectra of Nitrobenzene and Nitropyridines. *J. Appl. Spectrosc.* **2005**, *72*, 483−487.
(71) Hossain, M. Z.; Walsh, M. A.; Hersam, M. C. Scanning Tunneling Microscopy, Spectroscopy, and Nanolithography of Epitaxial Graphene Chemically Modified with Aryl Moieties. *J. Am. Chem. Soc.* **2010**, *132*, 15399−15403.
(72) Koehler, F. M.; Jacobsen, A.; Ensslin, K.; Stampfer, C.; Stark, W. J. Selective Chemical Modification of Graphene Surfaces: Distinction Between Single- and Bilayer Graphene. *Small* **2010**, *6*, 1125−1130.
(73) Farmer, D. B.; Golizadeh-Mojarad, R.; Perebeinos, V.; Lin, Y.-M.; Tulevski, G. S.; Tsang, J. C.; Avouris, P. Chemical Doping and Electron−Hole Conduction Asymmetry in Graphene Devices. *Nano Lett.* **2009**, *9*, 388−392.

https://doi.org/10.1021/acs.jpcc.2c05261
J. Phys. Chem. C 2022, 126, 17569−17578